

## Article

# Centennial-Scale Climatic Oscillations during the Dansgaard–Oeschger 14 Revealed by Stalagmite Isotopic Records from Shouyuangong Cave, Southern China

Shushuang Liu <sup>1,2</sup>, Zhenqiu Zhang <sup>2,3,\*</sup>, Xiumin Zhai <sup>2,4</sup>, Jianshun Chen <sup>2,3</sup>, Yuanhai Zhang <sup>4</sup>, Ping Long <sup>5</sup> and Zhiqiang Chen <sup>5</sup>

- <sup>1</sup> Shandong Provincial Key Laboratory of Water and Soil Conservation and Environmental Protection, School of Resources and Environment, Linyi University, Linyi 276000, China
- <sup>2</sup> School of Geography, Nanjing Normal University, Nanjing 210023, China
- <sup>3</sup> Key Laboratory of Virtual Geographic Environment (Nanjing Normal University), Ministry of Education, Nanjing 210023, China
- <sup>4</sup> Key Laboratory of Karst Dynamics, Institute of Karst Geology, Chinese Academy of Geological Sciences, Ministry of Natural Resources & Guangxi Zhuang Autonomous Region, Guilin 541004, China
- <sup>5</sup> Management Committee of Leye-Fengshan UNESCO Global Geopark, Baise 533200, China
- \* Correspondence: zhangzhenqiu@njnu.edu.cn

**Abstract:** During the last glacial, Dansgaard–Oeschger (DO) events are mostly characterized by moderate and shorter fluctuations. Here, we present the three-year-resolution stalagmite isotopic record from Shouyuangong Cave (SYG), southern China, revealing a detailed history of Asian summer monsoon (ASM) and local environmental changes during the middle and late period of DO 14. During this period, the SYG1  $\delta^{18}\text{O}$  is characterized by the persistence of centennial-scale oscillations. These centennial  $\delta^{18}\text{O}$  enrichment excursions are clearly mirrored in the  $\delta^{13}\text{C}$  signal. This correlation suggests that changes in soil  $\text{CO}_2$  production at this site are closely correlated with centennial-scale ASM variability. Furthermore, power spectrum analysis shows that  $\delta^{18}\text{O}$  and  $\delta^{13}\text{C}$  display the common periodicities consistent with solar activity cycles, implicating a control of solar activity on the ASM and soil humidity. Particularly, weak solar activity generally corresponds to weak ASM and a decline in soil  $\text{CO}_2$  production. One possible link between them is that external forcing controls the ASM intensity via the thermal contrast between the ocean and land. Subsequently, the balance of soil moisture co-varies with the hydrological responses. Finally, the soil  $\text{CO}_2$  production is further amplified by ecological effect.

**Keywords:** Shouyuangong Cave; centennial-scale variability; soil processes; solar activity



**Citation:** Liu, S.; Zhang, Z.; Zhai, X.; Chen, J.; Zhang, Y.; Long, P.; Chen, Z. Centennial-Scale Climatic Oscillations during the Dansgaard–Oeschger 14 Revealed by Stalagmite Isotopic Records from Shouyuangong Cave, Southern China. *Geosciences* **2022**, *12*, 400. <https://doi.org/10.3390/geosciences12110400>

Academic Editors: Pierre Pellenard, Xianglei Li, Yijia Liang and Jesus Martinez-Frias

Received: 26 September 2022

Accepted: 25 October 2022

Published: 27 October 2022

**Publisher's Note:** MDPI stays neutral with regard to jurisdictional claims in published maps and institutional affiliations.



**Copyright:** © 2022 by the authors. Licensee MDPI, Basel, Switzerland. This article is an open access article distributed under the terms and conditions of the Creative Commons Attribution (CC BY) license (<https://creativecommons.org/licenses/by/4.0/>).

## 1. Introduction

In the Marine Isotope Stage (MIS) 3, the Dansgaard–Oeschger (DO) events identified in the Greenland ice core are mostly characterized by moderate and shorter fluctuations [1]. Hence, few records are satisfactory to strictly constrain these DO events with sufficient resolution and robust age control [2]. The reasons for the internal structural changes are not clear, especially at centennial-scale oscillations [3,4]. Various hypotheses were invoked to explain these centennial-scale climate variations, including changes in the solar activity [5–8].

Changes in solar activity have previously been proposed to cause decadal- to millennial-scale fluctuations in both the Holocene and Last Glacial Maximum climates [7,9]. The good empirical evidence exists also for solar modulation of climate-related events on multi-decadal, centennial and bicentennial timescales [10–15]. Soon et al. [6] suggested strong empirical evidence supports the existence of sun–climate relationships on a number of centennial-to-millennial, suborbital timescales, and that these relationships are represented by climate proxy variations from nearly all the Earth's major climatic zones and regimes.

During the Holocene, the idea of solar forcing on climates was tested by comparison of decadal to centennial changes of the radionuclide proxies and geologic records [7,16–22]. Recently published high-resolution climate proxy records show that climate fluctuations in the LGM and Holocene are spectrally similar suggesting that linkages between climate proxies and solar activity at the centennial time scale in the Holocene can be extended to the LGM [8]. However, during the DO events, a connection between the solar activity and the centennial scale climate changes revealed by paleogeological records remains unclear due to insufficient data resolution and age controls. Therefore, the decadal to centennial-scale Asian summer monsoon (ASM) instability during the DO events (i.e., intra-DO) still needs to be further investigated, as this type of climate oscillation is in frequency similar to the solar cycles and is likely instrumental in testing the hypothesis of solar forcing on the DO events.

Here we present the 3-year-resolution stalagmite isotopic records of DO 14 from Shouyuangong cave, which has allowed us to scrutinize the decadal- to centennial-scale variability of the ASM and local environments.

## 2. Cave Site, Sample, and Methods

Shouyuangong Cave ( $24^{\circ}25' N$ ,  $107^{\circ}01' E$ , 667 m above sea level) is located in the zone of transition between Yun-Gui Plateau to Guangxi Basin, southern China (Figure 1a). The entrance of the cave is 20 m wide and 12 m high. The plane of the cave is asymmetrical and skewed in the shape of Y. The cave is about 4062 m long with six chambers (Figure 1b). The regional climate condition is influenced by the subtropical east Asian and tropical Indian summer monsoons. Mean annual temperature is about  $16\text{--}19^{\circ}C$  and the annual precipitation is about 1500–1600 mm.

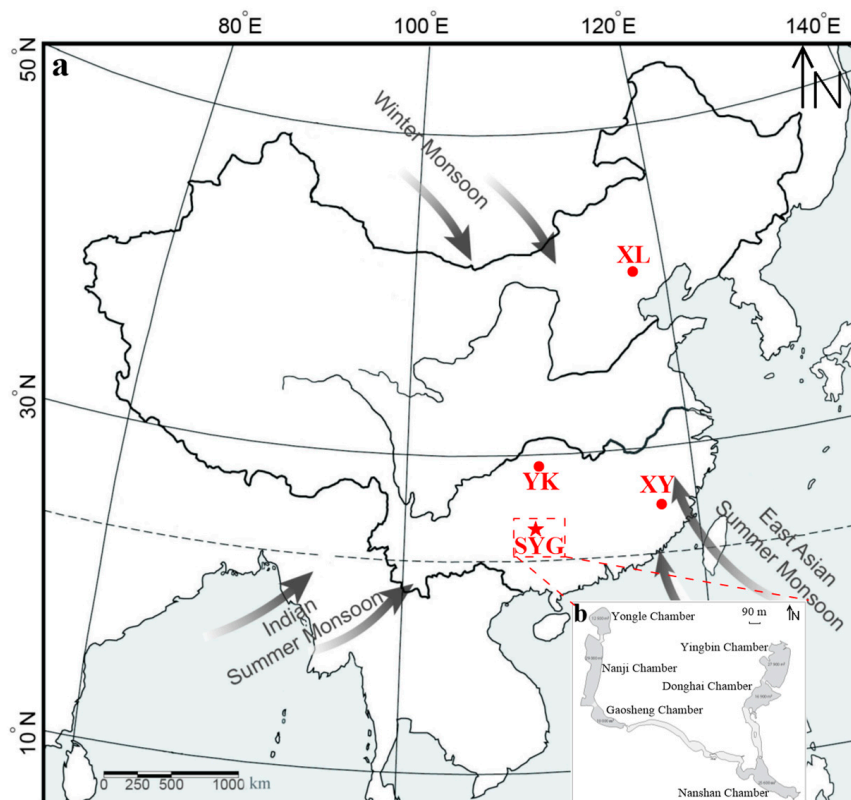


**Figure 1.** Regional climatology, cave sites (a) and the plan of Shouyuangong Cave (b). Averaged JJA water vapor flux between 1949 and 2016 [22]. Red dots indicate locations of Xinglong Cave (XL,  $40^{\circ}29' N$ ,  $117^{\circ}29' E$ , [23]), Yangkou Cave (YK,  $29^{\circ}01' N$ ,  $107^{\circ}11' E$ , [24]) and Xianyun cave (XY,  $25^{\circ}33' N$ ,  $117^{\circ}00' E$ , [25]). Red star indicates location of Shouyuangong Cave (SYG,  $24^{\circ}25' N$ ,  $107^{\circ}01' E$ , this study).

Stalagmite SYG1 is 980 mm in length with a candlestick shape and has a diameter of 250 mm (Figure 2), suggesting the infiltration water feeding the stalagmite was generally stable. When halved and polished, SYG1 is composed of translucent and porous calcite (Figure 2). Lithological features of this sample can be divided into two phases with a 645 mm boundary. In the upper 645 mm, the polished section is composed of milk-white calcite and transparent and compact calcite can be observed below this zone (Figure 2).

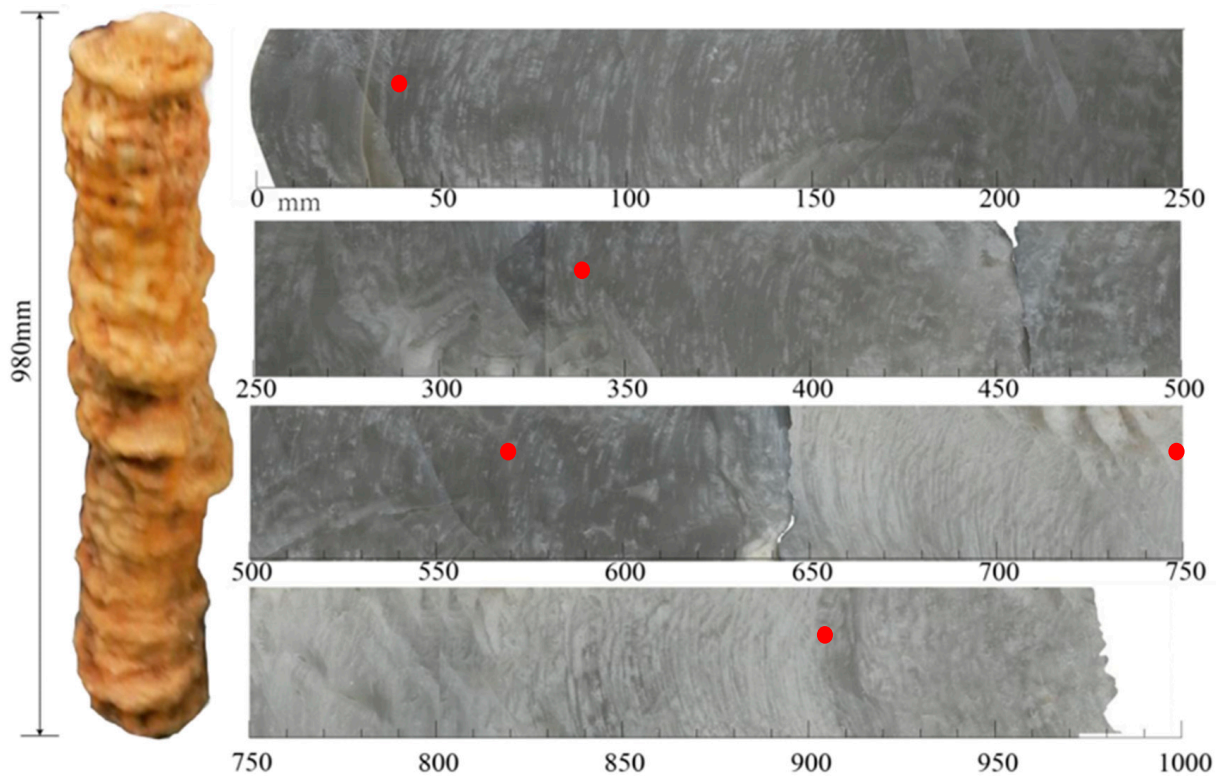


**Figure 2.** Photograph of stalagmite SYG1 from Shouyuangong Cave. The red dots indicate layers for  $^{230}\text{Th}/\text{U}$  dating.

In order to ensure that the dating points were evenly distributed in depth, an age point was collected every 200 mm or so. Therefore, five powder sub-samples were collected along the growth axis using 0.9-mm-diameter carbide dental burrs for  $^{230}\text{Th}$  dating. Measurements were performed on a Neptune MC-ICP-MS at the School of Geography, Nanjing Normal University. The chemical procedure used to separate uranium and thorium is similar to those described in Shao et al. [26]. The U and Th isotopic measurements and data processing followed Shao et al. [27]. 392 sub-samples were drilled for stable isotopic measurements using 0.3 mm-diameter carbide dental burrs. Analyses were performed on a Finnigan-MAT 253 mass spectrometer fitted with a Kiel Carbonate Device at the School of Geography, Nanjing Normal University. The results were reported relative to Vienna Pee Dee Belemnite (VPDB) with standardization determined relative to NBS 19. Precision of  $\delta^{18}\text{O}$  values is 0.06‰ and 0.03‰ for  $\delta^{13}\text{C}$ , at  $1\sigma$  level.

### 3. Results

#### 3.1. Chronology

$^{230}\text{Th}$  dates reveal that the growth of stalagmite SYG1 covered a period from 52.7 to 50.0 ka and increase systematically with depth from the top (Table 1). The typical analytical errors ( $2\sigma$ ) of dating results are generally less than 190 years. The average U concentration throughout the stalagmite is 0.1 ppm and  $^{232}\text{Th}$  content is low (generally less than 280 ppt).  $^{232}\text{Th}$  dates were linearly interpolated to establish chronologies (Figure 3a). In the Figure 2, the color of calcite changes markedly at 645 mm. Therefore, we use an algorithmic method, StalAge [28] to test whether there were hiatuses, and large changes in growth rate. As a

result, the modeled ages generally agreed within the 95% confidence level, with linearly interpolated chronologies between adjacent  $^{230}\text{Th}$  ages. Hence, SYG1 is a linear rate of growth without depositional discontinuities.

**Table 1.**  $^{230}\text{Th}$  dating results of stalagmite SYG1 from southern China.

Sample Number	Depth (mm)	$^{238}\text{U}$ (ppb)	$^{232}\text{Th}$ (ppt)	$\delta^{234}\text{U}$ (‰) (Measured)	$^{230}\text{Th}/^{238}\text{U}$ ( $10^{-3}$ ) (Activity)	$^{230}\text{Th}/^{232}\text{Th}$ (Activity)	$^{230}\text{Th}$ Age (ka) (Uncorrected)	$^{230}\text{Th}$ Age (ka) (Corrected)	$\delta^{234}\text{U}_{\text{initial}}$ (‰) (Corrected)
SYG1-40	40	119.37 ± 0.04	279.9 ± 10.0	25.9 ± 1.0	379.4 ± 0.7	494.5 ± 17.7	50.2 ± 0.1	50.1 ± 0.1	29.9 ± 1.6
SYG1-340	340	123.15 ± 0.05	212.3 ± 10.0	28.0 ± 1.1	383.6 ± 0.7	680.2 ± 32.0	50.7 ± 0.1	50.7 ± 0.1	32.2 ± 1.2
SYG1-570	570	132.03 ± 0.04	205.3 ± 10.1	28.8 ± 1.0	388.5 ± 0.7	763.5 ± 37.4	51.5 ± 0.1	51.5 ± 0.1	33.4 ± 1.1
SYG1-750	750	125.17 ± 0.04	257.1 ± 10.1	27.9 ± 1.1	390.0 ± 0.7	580.2 ± 22.5	51.8 ± 0.1	51.8 ± 0.1	32.3 ± 1.2
SYG1-905	905	91.48 ± 0.03	153.6 ± 10.2	29.3 ± 1.4	394.4 ± 0.9	717.7 ± 47.8	52.4 ± 0.2	52.4 ± 0.2	34.0 ± 1.7

Errors are  $2\sigma$  analytical errors. Decay constant values are  $\lambda_{230} = 9.1577 \times 10^{-6} \text{ yr}^{-1}$  [29],  $\lambda_{234} = 2.8263 \times 10^{-6} \text{ yr}^{-1}$  [30],  $\lambda_{238} = 1.55125 \times 10^{-10} \text{ yr}^{-1}$  [30]. Corrected  $^{230}\text{Th}$  ages assume an initial  $^{230}\text{Th}/^{232}\text{Th}$  atomic ratio of  $(4.4 \pm 2.2) \times 10^{-6}$ . Corrected  $^{230}\text{Th}$  ages are indicated in bold, and presented in thousand years before 1950 AD.

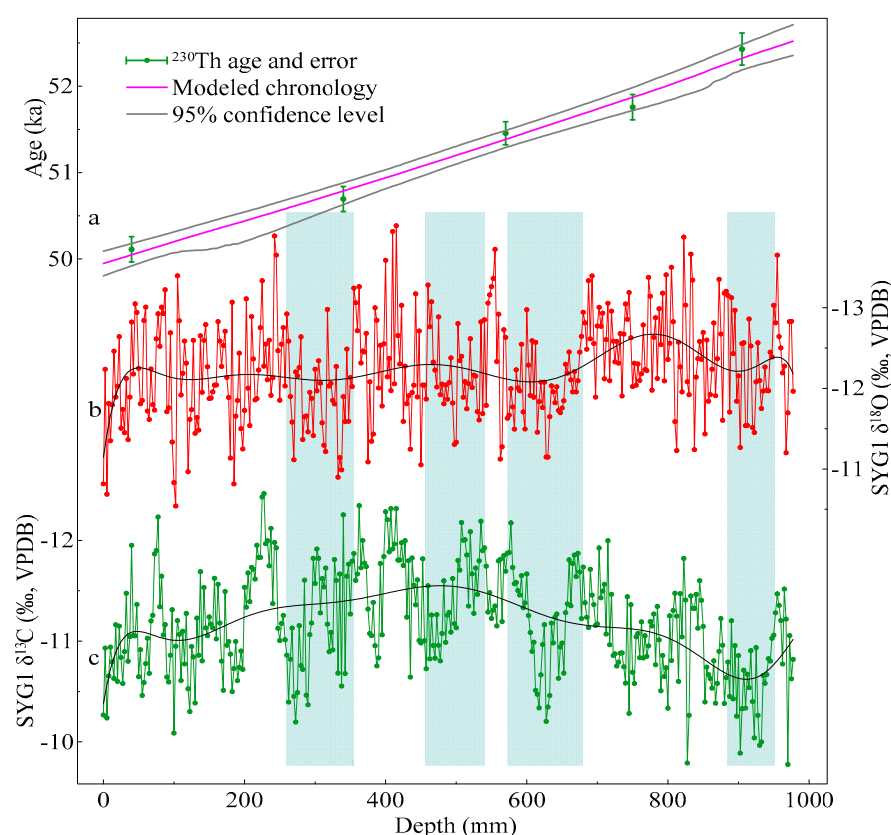


**Figure 3.** The age model (a),  $\delta^{18}\text{O}$  (b) and  $\delta^{13}\text{C}$  (c) isotopic sequences for Sample SYG1. The age–depth relation of SYG1 was reconstructed by a linear interpolation between adjacent dates, with error bars showing the dating uncertainties. Pink and gray lines denote the modeled age and 95% confidence level. Green dots and bars show dating results and errors. The red and green lines and dots represent  $\delta^{18}\text{O}$  (b) and  $\delta^{13}\text{C}$  (c), respectively. The solid black line shows the polynomial fitting of stalagmite SYG1  $\delta^{18}\text{O}$  and  $\delta^{13}\text{C}$ . The light blue bars label the coeval isotopic enrichment.

### 3.2. Oxygen and Carbon Isotope Records

During the growth period, the  $\delta^{18}\text{O}$  is characterized by persistence of centennial-scale oscillations around the mean  $-12.2\text{‰}$ , supporting by the polynomial fitting of the  $\delta^{18}\text{O}$  record with four centennial-scale oscillations (Figure 3b). Between 51.7 ka and 51.4 ka, large-amplitude (2‰) and centennial-scale fluctuations are evident in the  $\delta^{18}\text{O}$  (Figure 3b). In the Figure 3b, interestingly, the SYG1  $\delta^{13}\text{C}$  is superimposed with a series of secondary oscillations (Figure 3c), corresponding to  $\delta^{18}\text{O}$ .

Temporally, the growth of SYG1 covered a period from the middle and late period of DO 14. The DO 14 in SYG1  $\delta^{18}\text{O}$  is synchronous with the Yangkou [24] (Figure 4b), Xinglong record [23] (Figure 4c) and Xianyun [25] (Figure 4d) within dating errors, especially the most evident centennial-scale enrichment excursions (light blue bar in Figure 4) indicating the accuracy of the stalagmite SYG1 dating. As previously suggested, the Chinese stalagmite  $\delta^{18}\text{O}$  records are dynamically linked to rainfall isotopic composition associated with changes of the ASM intensity [31,32]. Thus, the observed similarity between these speleothem  $\delta^{18}\text{O}$  records over broad regions implies that they are of climatic origin and SYG1  $\delta^{18}\text{O}$  signal can represent a regional climate response, i.e., ASM variability [33,34], with minimum values corresponding to a strong ASM.

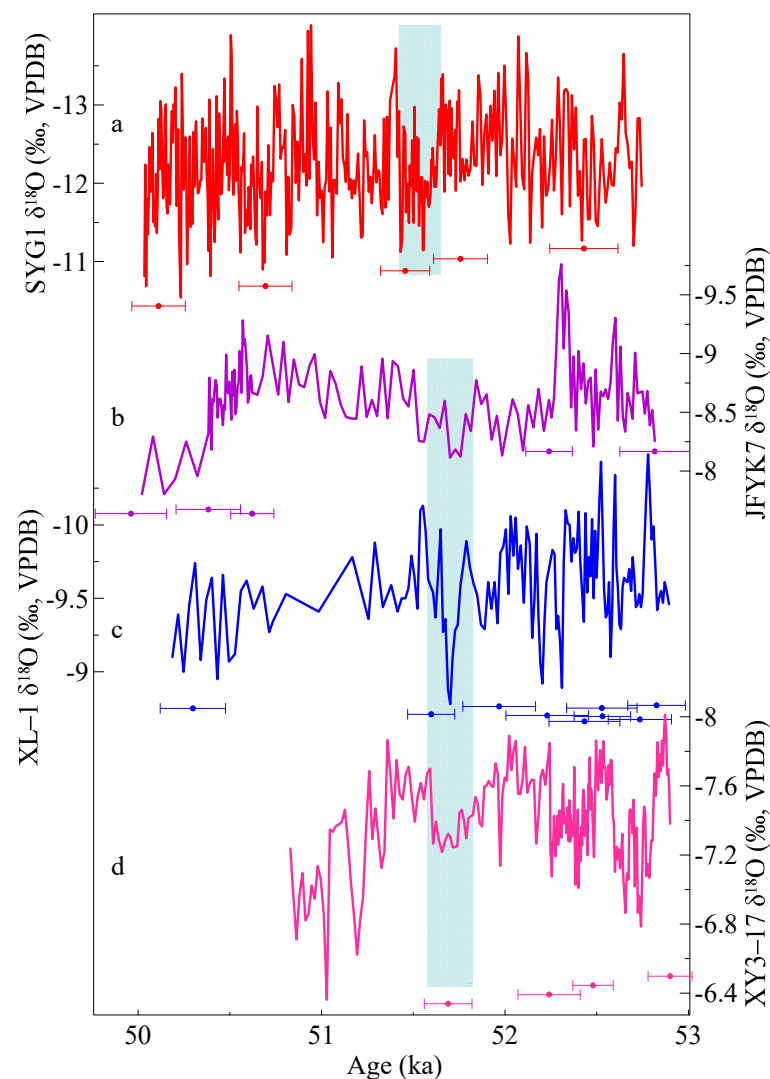


**Figure 4.** Comparison of our  $\delta^{18}\text{O}$  record with other Chinese speleothem records. From the top to bottom are (a) SYG1  $\delta^{18}\text{O}$  (red line, this study) and (b)  $\delta^{18}\text{O}$  record from Yangkou Cave [24] (purple line), (c)  $\delta^{18}\text{O}$  record from Xinglong cave [23] (blue line) and (d)  $\delta^{18}\text{O}$  record from Xianyun Cave [25] (pink line). The light blue bar denotes the most evident centennial-scale fluctuations.

## 4. Discussion

### 4.1. Centennial-Scale Coupling of ASM and Soil Processes

We note that the millennial-scale  $\delta^{18}\text{O}$  variability is superimposed by a series of minor oscillations (about 1‰ in amplitude) supported by the polynomial fitting of the  $\delta^{18}\text{O}$  record (Figure 3a). These centennial  $\delta^{18}\text{O}$  enrichment excursions are clearly mirrored in the  $\delta^{13}\text{C}$  signal (light blue bar in Figure 3). This correlation indicates that centennial-scale

$\delta^{13}\text{C}$  variations might be associated with moisture changes. During the growth period, power spectrum analysis [35] shows that the SYG1  $\delta^{18}\text{O}$  exhibits statistically significant periodicities centered on 240 a, 171 a and 144 a (above 99% confidence level, Figure 5a,b). And the periods of  $\delta^{13}\text{C}$  are 452 a, 241a, 164 a, and 145 a (above 99% confidence level, Figure 5b). Therefore, SYG1  $\delta^{18}\text{O}$  and  $\delta^{13}\text{C}$  display the same periods above 99% confidence level except 452 a for  $\delta^{13}\text{C}$  (Figure 5a,b). This tight link indicates that centennial-scale changes of both isotopic signals might have the same forcing mechanism and/or the climatic and environmental changes influence them in the same direction.

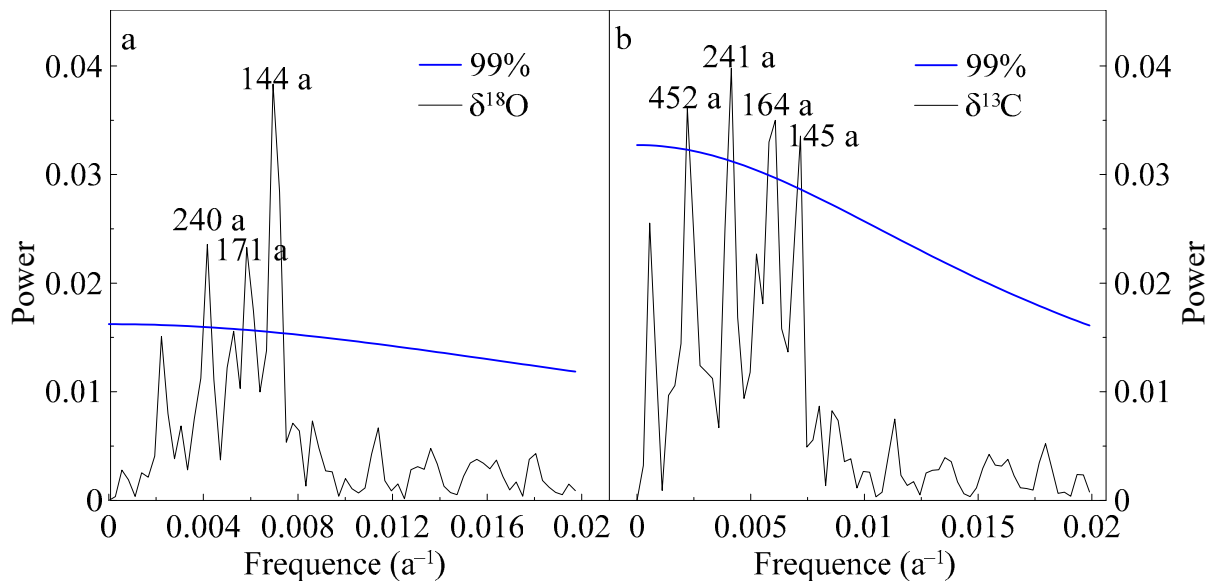


**Figure 5.** REDFIT spectral analysis of SYG1  $\delta^{18}\text{O}$  (a) and  $\delta^{13}\text{C}$  (b) by using the software program Past3 [35]. The solid blue line represent 99% confidence level.

Given the soil  $\text{CO}_2$  concentration is about 10–100 times that of the atmosphere [36], and about 80–90% of carbon in stalagmites is derived from the soil  $\text{CO}_2$  [37], the biogenic  $\text{CO}_2$  production in the soil associated with the plant respiration and microbiological decomposition possibly has a significant impact on the speleothem  $\delta^{13}\text{C}$  signal. The warming and wetting climate conditions will promote the biological activity, and hence enhance the soil  $\text{CO}_2$  production. Generally, the isotopic composition of biogenic soil  $\text{CO}_2$  is depleted in  $^{13}\text{C}$  [38], with a high soil  $\text{CO}_2$  partial pressure ( $\rho\text{CO}_2$ ) corresponding to low  $\delta^{13}\text{C}$  values [39]. This isotopic signal can be reflected in the speleothems deposited in the cave [37,40]. In the Figure 3, the decrease of soil  $\text{CO}_2$  production (increase in the calcite  $\delta^{13}\text{C}$ ) closely follows the rapid ASM decline. This relationship indicates a dominant role of water availability on our speleothem  $\delta^{13}\text{C}$  records. Thus, centennial-scale  $\delta^{13}\text{C}$  variability at this site is, to some degree, controlled by regional hydrological circulations, possibly via the local soil humidity level [41].

#### 4.2. Forcing Mechanisms of Centennial-Scale Oscillations

During the growth period, SYG1  $\delta^{18}\text{O}$  and  $\delta^{13}\text{C}$  reveal the common periodicities (240 a, 171 a and 144 a for  $\delta^{18}\text{O}$ ; 241a, 164 a and 145 a for  $\delta^{13}\text{C}$ ) above 99% confidence level (Figure 5a,b). Moreover, these periods are similar to solar cycles 228 a, 169 a and 136 a [9,42], reflecting the imprint of solar activity on the East Asian monsoon. Additionally, periods of weak ASM (increase in the  $\delta^{18}\text{O}$ ) (Figure 6a) and decline in the soil  $\text{CO}_2$  production (enrichment of  $\delta^{13}\text{C}$ ) (Figure 6b) are generally consistent with decrease of solar output [43] (Figure 6c), pointing to a common mechanism on changes of the ASM and karstic processes, potentially associated with the solar output.

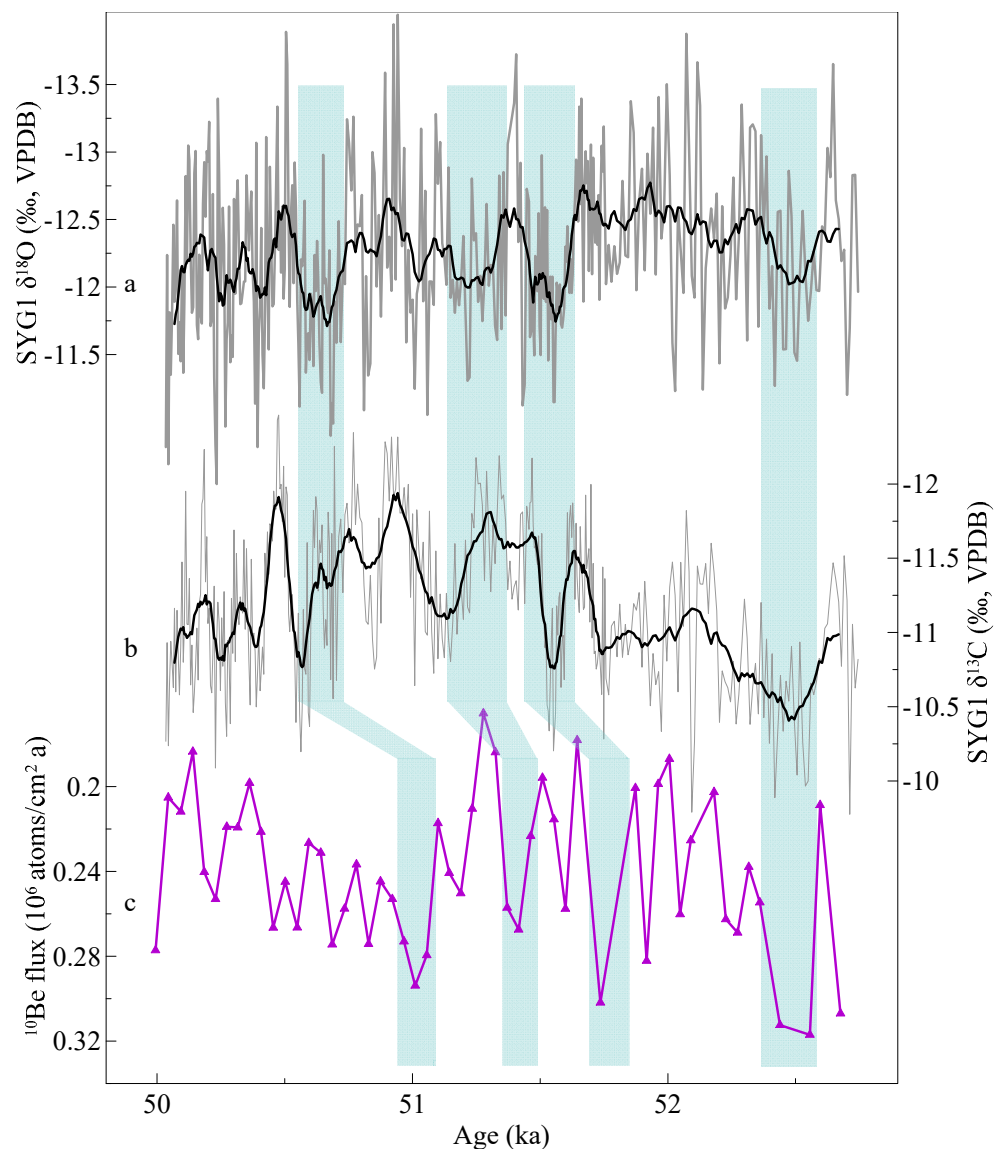


**Figure 6.** Correlation of centennial-scale changes in (a) the SYG1  $\delta^{18}\text{O}$  (gray line) and (b)  $\delta^{13}\text{C}$  records (gray line), and (c)  $^{10}\text{Be}$  flux from GRIP and GISP2 ice cores [43] (purple line). The black line indicates a 15-point running average of the stalagmite XYG1  $\delta^{18}\text{O}$  and  $\delta^{13}\text{C}$  record. Light blue bars indicate synchronous changes in these records.

Typically, the carbon isotopes are incorporated into the speleothem as dissolved inorganic carbon (DIC). The dominant DIC species is bicarbonate ( $\text{HCO}_3^-$ ), the initial isotopic signal of which is strongly impacted by soil  $\text{CO}_2$ , soil-respired  $\text{CO}_2$  and degradation of soil organic matter (SOM) [37]. It was believed that the soil temperature and humidity are prominent limiting factors for vegetation growth, soil organic matter decomposition, microorganism activity and root respiration [44]. Therefore, the observed centennial-scale co-variation between  $\delta^{18}\text{O}$  and  $\delta^{13}\text{C}$  records and solar proxies implies a control of solar activity on the ASM circulation (regional) and site-specific soil humidity (local).

High-resolution stalagmite records show that solar activity played an important role in driving centennial scale climatic oscillation during the Holocene [7]. Within our error range (about 150 a), the record shows the centennial-scale changes in the calcite record appear to be consistent with the solar activity variations [43] (Figure 6). The  $^{10}\text{Be}$  flux increased significantly, which corresponded to the enrichment excursions of SYG1  $\delta^{18}\text{O}$  and  $\delta^{13}\text{C}$  (Figure 6), indicating weak solar activity generally corresponds to weak ASM and a decline in soil  $\text{CO}_2$  production.

Bond et al. [17] pointed out that the influence of solar activity on global climate change is amplified through thermohaline circulation. In terms of monsoon dynamics, solar activity can directly affect monsoon by affecting the thermal differences between land and sea [45,46]. Our comparison shows that centennial-scale solar variability is possibly an interpretation of regional climate and soil humidity changes across the DO events. One possible link between them is that external forcing controls the ASM intensity via the thermal contrast between the ocean and land. Subsequently, the balance of soil moisture co-varies with the hydrological responses. Finally, the soil CO<sub>2</sub> production is further amplified by ecological effects.

## 5. Conclusions

The three-year resolved speleothem records of  $\delta^{18}\text{O}$  (representing the ASM variability) and  $\delta^{13}\text{C}$  (reflecting changes of soil CO<sub>2</sub> production) reconstruct a history of the ASM and environmental changes in the middle and late period of DO 14 from Shouyuangong Cave, southern China. During the growth period, persistent centennial-scale oscillations are clear in the  $\delta^{18}\text{O}$  record, especially at 51.7 and 51.4 ka. The  $\delta^{13}\text{C}$  shows a decreasing trend superimposed with a series of secondary oscillations. Interestingly, minor centennial-scale oscillations in the  $\delta^{18}\text{O}$  record are well reflected in the  $\delta^{13}\text{C}$  signal, and both correlate well with the solar activity. Power spectrum analysis shows that SYG1  $\delta^{18}\text{O}$  and  $\delta^{13}\text{C}$  display the same periods, consistent with solar activity cycles, implicating the control of solar activity over the ASM and soil humidity. Moreover, periods of weak ASM (increase in the  $\delta^{18}\text{O}$ ) and decline in the soil CO<sub>2</sub> production (enrichment of  $\delta^{13}\text{C}$ ) are generally consistent with decreases in solar output. This correspondence indicates that the site-specific moisture level is of importance for the soil CO<sub>2</sub> production, both of which are probably related to centennial-scale solar activity. One possible link between them is that external forcing controls the ASM intensity via the thermal contrast between the ocean and land. Of course, at centennial scale, the solar activity forcing on the East Asian summer monsoon was further confirmed with more high-resolution records.

**Author Contributions:** Conceptualization, S.L. and Z.Z.; Funding acquisition, Z.Z.; Investigation, X.Z., Y.Z., P.L. and Z.C.; Methodology, S.L. and J.C.; Writing—original draft, S.L.; Writing—review & editing, Z.Z. and S.L. All authors have read and agreed to the published version of the manuscript.

**Funding:** This research was funded by grants from the National Natural Science Foundation of China (grant number 42202213) and the Open Fund of Leye-Fengshan UNESCO Global Geopark (grant number LFD20001).

**Data Availability Statement:** Data are available on request.

**Acknowledgments:** We are thankful to the National Natural Science Foundation of China (grant number 42202213) and the Open Fund of Leye-Fengshan UNESCO Global Geopark (grant number LFD20001). In addition, we thank the Management Committee of Leye-Fengshan UNESCO Global Geopark, Guangxi, China.

**Conflicts of Interest:** The authors declare no conflict of interest.

## References

1. Hinnov, L.A.; Schulz, M.; Yiou, P. Interhemispheric Space–Time Attributes of the Dansgaard–Oeschger Oscillations between 100 and 0 Ka. *Quat. Sci. Rev.* **2002**, *21*, 1213–1228. [[CrossRef](#)]
2. Voelker, A.H.L. Global Distribution of Centennial-Scale Records for Marine Isotope Stage (MIS) 3: A Database. *Quat. Sci. Rev.* **2002**, *21*, 1185–1212. [[CrossRef](#)]
3. Jiang, X.; He, Y.; Wang, X.; Dong, J.; Li, Z.; Lonee, M.A.; Shen, C.-C. Journal of Asian Earth Sciences Sub-Decadally-Resolved Asian Monsoon Dynamics during Chinese Interstadial 21 in Response to Northern High-Latitude Climate. *J. Asian Earth Sci.* **2019**, *172*, 243–248. [[CrossRef](#)]
4. Liu, S.; Liu, D.; Wang, Y.; Shao, Q.; Liang, Y.; Gao, H.; Mi, X. Insolation Control of Millennial-Scale Asian Summer Monsoon Changes Evidenced by Chinese Stalagmites  $\delta^{18}\text{O}$  Records. *Quat. Int.* **2022**, *616*, 30–39. [[CrossRef](#)]

5. Dykoski, C.A.; Edwards, R.L.; Cheng, H.; Yuan, D.; Cai, Y.; Zhang, M.; Lin, Y.; Qing, J.; An, Z.; Revenaugh, J. A High-Resolution, Absolute-Dated Holocene and Deglacial Asian Monsoon Record from Dongge Cave, China. *Earth Planet. Sci. Lett.* **2005**, *233*, 71–86. [[CrossRef](#)]
6. Soon, W.; Velasco Herrera, V.M.; Selvaraj, K.; Traversi, R.; Usoskin, I.; Chen, C.T.A.; Lou, J.Y.; Kao, S.J.; Carter, R.M.; Pipin, V.; et al. A Review of Holocene Solar-Linked Climatic Variation on Centennial to Millennial Timescales: Physical Processes, Interpretative Frameworks and a New Multiple Cross-Wavelet Transform Algorithm. *Earth Sci. Rev.* **2014**, *134*, 1–15. [[CrossRef](#)]
7. Wang, Y.; Cheng, H.; Edwards, R.L.; He, Y.; Kong, X.; An, Z.; Wu, J.; Kelly, M.; Dykoski, C.A.; Li, X. Changes and North Atlantic Climate The Holocene Asian Monsoon: Links to Solar Changes and North Atlantic Climate. *Science* **2008**, *303*, 854–857. [[CrossRef](#)]
8. Kravchinsky, V.A.; Zhang, R.; Borowiecki, R.; Tarasov, P.E.; Van Der Baan, M.; Anwar, T.; Goguitchaichvili, A.; Müller, S. Centennial Scale Climate Oscillations from Southern Siberia in the Last Glacial Maximum. *Quat. Sci. Rev.* **2021**, *270*, 107171. [[CrossRef](#)]
9. Adolphi, F.; Muscheler, R.; Svensson, A.; Aldahan, A.; Possnert, G.; Beer, J.; Sjolte, J.; Björck, S.; Matthes, K.; Thiéblemont, R. Persistent Link between Solar Activity and Greenland Climate during the Last Glacial Maximum. *Nat. Geosci.* **2014**, *7*, 662–666. [[CrossRef](#)]
10. Van Loon, H.; Brown, J.; Milliff, R.F. Trends in Sunspots and North Atlantic Sea Level Pressure. *J. Geophys. Res.* **2012**, *117*, D07106. [[CrossRef](#)]
11. Soon, W.W. Solar Arctic-Mediated Climate Variation on Multidecadal to Centennial Timescales: Empirical Evidence, Mechanistic Explanation, and Testable Consequences. *Phys. Geogr.* **2009**, *30*, 144–184. [[CrossRef](#)]
12. Soon, W.; Dutta, K.; Legates, D.R.; Velasco, V.; Zhang, W. Journal of Atmospheric and Solar-Terrestrial Physics Variation in Surface Air Temperature of China during the 20th Century. *J. Atmos. Sol.-Terr. Phys.* **2011**, *73*, 2331–2344. [[CrossRef](#)]
13. Soon, W.; Legates, D.R. Journal of Atmospheric and Solar-Terrestrial Physics Solar Irradiance Modulation of Equator-to-Pole (Arctic) Temperature Gradients: Empirical Evidence for Climate Variation on Multi-Decadal Timescales. *J. Atmos. Sol.-Terr. Phys.* **2013**, *93*, 45–56. [[CrossRef](#)]
14. Weng, H. Impacts of Multi-Scale Solar Activity on Climate. Part II: Dominant Timescales in Decadal-Centennial Climate Variability. *Adv. Atmos. Sci.* **2012**, *29*, 887–908. [[CrossRef](#)]
15. Weng, H. Impacts of Multi-Scale Solar Activity on Climate. Part I: Atmospheric Circulation Patterns and Climate Extremes. *Adv. Atmos. Sci.* **2012**, *29*, 867–886. [[CrossRef](#)]
16. Marchitto, T.M.; Muscheler, R.; Ortiz, J.D.; Carriquiry, J.D.; Van Geen, A.; Carriquiry, J.D.; Geen, A. Van Holocene Linked References Are Available on JSTOR for This Article: Dynamical Response of the Tropical Pacific Ocean to Solar Forcing During the Early Holocene. *Geophys. Res. Lett.* **2016**, *330*, 1378–1381.
17. Bond, G.; Kromer, B.; Beer, J.; Muscheler, R.; Evans, M.N.; Showers, W.; Hoffmann, S.; Lotti-Bond, R.; Hajdas, I.; Bonani, G. Persistent Solar Influence on North Atlantic Climate during the Holocene. *Science* **2001**, *294*, 2130–2136. [[CrossRef](#)]
18. Fleitmann, D.; Burns, S.J.; Mudelsee, M.; Neff, U.; Mangini, A.; Matter, A.; Fleitmann, D.; Burns, S.J.; Mudelsee, M.; Neff, U.; et al. Holocene Forcing of the Indian Monsoon Recorded in a Stalagmite from Southern Oman. *Science* **2016**, *300*, 1737–1739. Available online: <http://www.jstor.org/stable/3834589> (accessed on 18 September 2016). [[CrossRef](#)]
19. Gupta, A.K.; Das, M.; Anderson, D.M. Solar Influence on the Indian Summer Monsoon during the Holocene. *Geophys. Res. Lett.* **2005**, *32*, 2–5. [[CrossRef](#)]
20. Hu, F.S.; Kaufman, D.; Yoneji, S.; Nelson, D.; Shemesh, A.; Huang, Y.; Tian, J.; Bond, G.; Clegg, B.; Brown, T. Cyclic Variation and Solar Forcing of Holocene Climate in the Alaskan Subarctic. *Science* **2016**, *301*, 1890–1893. Available online: <http://www.jstor.org/stable/3835182> (accessed on 20 September 2016). [[CrossRef](#)]
21. Neff, U.; Burus, S.; Mangini, A.; Mudelsee, M.; Fleitmann, D.; Matter, A. Strong Coherence between Solar Variability and the Monsoon in Oman between 9 and 6 Kyr Ago. *Nature* **2001**, *411*, 290–293. [[CrossRef](#)] [[PubMed](#)]
22. Schmidt, M.W.; Weinlein, W.A.; Marcantonio, F.; Lynch-stieglitz, J. Solar Forcing of Florida Straits Surface Salinity during the Early Holocene. *Paleoceanography* **2012**, *27*, PA3204. [[CrossRef](#)]
23. Duan, W.; Cheng, H.; Tan, M.; Edwards, R.L. Onset and Duration of Transitions into Greenland Interstadials 15.2 and 14 in Northern China Constrained by an Annually Laminated Stalagmite. *Sci. Rep.* **2016**, *6*, 20844. [[CrossRef](#)]
24. Li, T.Y.; Han, L.; Cheng, H.; Edwards, R.L.; Shen, C.C.; Li, H.; Li, J.; Huang, C.; Zhang, T.; Zhao, X. Evolution of the Asian Summer Monsoon during Dansgaard/Oeschger Events 13–17 Recorded in a Stalagmite Constrained by High-Precision Chronology from Southwest China. *Quat. Res.* **2017**, *88*, 121–128. [[CrossRef](#)]
25. Zhang, X.; Jiang, X.; Xiao, H.; Cai, B.; Yu, T.L.; Shen, C.C. A Gradual Transition into Greenland Interstadial 14 in Southeastern China Based on a Sub-Decadally-Resolved Stalagmite Record. *Quat. Sci. Rev.* **2021**, *253*, 106769. [[CrossRef](#)]
26. Shao, Q.; Pons-branchu, E.; Zhu, Q.; Wang, W.; Fontugne, M. High Precision U/Th Dating of the Rock Paintings at Mt. Huashan. *Quat. Res.* **2017**, *88*, 1–13. [[CrossRef](#)]
27. Shao, Q.F.; Li, C.H.; Huang, M.J.; Liao, Z.B.; Arps, J.; Huang, C.Y.; Chou, Y.C.; Kong, X.G. Interactive Programs of MC-ICPMS Data Processing for <sup>230</sup>Th/U Geochronology. *Quat. Geochronol.* **2019**, *51*, 43–52. [[CrossRef](#)]
28. Scholz, D.; Hoffmann, D.L. StalAge—An Algorithm Designed for Construction of Speleothem Age Models. *Quat. Geochronol.* **2011**, *6*, 369–382. [[CrossRef](#)]
29. Jaffey, A.H.; Flynn, K.F.; Glendenin, L.E.; Bentley, W.C.; Essling, A.M. Precision Measurement of Half-Lives and Specific Activities of U<sup>235</sup> and U<sup>238</sup>. *Phys. Rev. C* **1971**, *4*, 1889–1906. [[CrossRef](#)]

30. Cheng, H.; Lawrence Edwards, R.; Shen, C.C.; Polyak, V.J.; Asmerom, Y.; Woodhead, J.; Hellstrom, J.; Wang, Y.; Kong, X.; Spötl, C.; et al. Improvements in  $^{230}\text{Th}$  Dating,  $^{230}\text{Th}$  and  $^{234}\text{U}$  Half-Life Values, and U-Th Isotopic Measurements by Multi-Collector Inductively Coupled Plasma Mass Spectrometry. *Earth Planet. Sci. Lett.* **2013**, *371–372*, 82–91. [[CrossRef](#)]
31. Cheng, H.; Sinha, A.; Wang, X.; Cruz, F.W.; Edwards, R.L. The Global Paleomonsoon as Seen through Speleothem Records from Asia and the Americas. *Clim. Dyn.* **2012**, *39*, 1045–1062. [[CrossRef](#)]
32. Tan, M. Circulation Effect: Response of Precipitation  $\delta^{18}\text{O}$  to the ENSO Cycle in Monsoon Regions of China. *Clim. Dyn.* **2013**, *42*, 1067–1077. [[CrossRef](#)]
33. Wang, Y.J.; Cheng, H.; Edwards, R.L.; An, Z.S.; Wu, J.Y.; Shen, C.-C.; Dorale, J.A. A High-Resolution Absolute-Dated Late Pleistocene Monsoon Record from Hulu Cave, China. *Science* **2012**, *2345*, 2345–2348. [[CrossRef](#)] [[PubMed](#)]
34. Cheng, H.; Edwards, R.L.; Sinha, A.; Spötl, C.; Yi, L.; Chen, S.; Kelly, M.; Kathayat, G.; Wang, X.; Li, X.; et al. 640,000 Years and Ice Age Terminations. *Nature* **2016**, *534*, 640–646. [[CrossRef](#)]
35. Schulz, M.; Mudelsee, M. REDFIT: Estimating Red-Noise Spectra Directly from Unevenly Spaced Paleoclimatic Time Series. *Comput. Geosci.* **2002**, *28*, 421–426. [[CrossRef](#)]
36. Andrews, J.A.; Schlesinger, W.H. Soil  $\text{CO}_2$  Dynamics, Acidification, and Chemical Weathering in a Temperature Forest with Experimental  $\text{CO}_2$  Enrichment. *Glob. Biogeochem. Cycles* **2001**, *15*, 149–162. [[CrossRef](#)]
37. Genty, D.; Baker, A.; Massault, M.; Proctor, C.; Gilmour, M.; Pons-Branchu, E.; Hamelin, B. Dead Carbon in Stalagmites: Carbonate Bedrock Paleodissolution vs. Ageing of Soil Organic Matter. Implications for  $^{13}\text{C}$  Variations in Speleothems. *Geochim. Cosmochim. Acta* **2001**, *65*, 3443–3457. [[CrossRef](#)]
38. Cerling, T.E.; Solomon, D.K.; Quade, J.; Bowman, J.R. On the Isotopic Composition of Carbon in Soil Carbon Dioxide. *Geochim. Cosmochim. Acta* **1991**, *55*, 3403–3405. [[CrossRef](#)]
39. Keeling, C.; Mook, W.; Tans, P. Recent Trends in the  $^{13}\text{C}/^{12}\text{C}$  Ratio of Atmospheric Carbon Dioxide. *Nature* **1979**, *277*, 121–123. [[CrossRef](#)]
40. Blyth, A.J.; Smith, C.I.; Drysdale, R.N. A New Perspective on the  $\Delta^{13}\text{C}$  Signal Preserved in Speleothems Using LC-IRMS Analysis of Bulk Organic Matter and Compound Specific Stable Isotope Analysis. *Quat. Sci. Rev.* **2013**, *75*, 143–149. [[CrossRef](#)]
41. Liu, D.; Wang, Y.; Cheng, H.; Edwards, R.L.; Kong, X.; Li, T.Y. Strong Coupling of Centennial-Scale Changes of Asian Monsoon and Soil Processes Derived from Stalagmite  $\delta^{18}\text{O}$  and  $\delta^{13}\text{C}$  Records, Southern China. *Quat. Res.* **2016**, *85*, 333–346. [[CrossRef](#)]
42. Damon, P.E.; Peristykh, A.N. Radiocarbon Calibration and Application to Geophysics, Solar Physics, and Astrophysics. *Radiocarbon* **2000**, *42*, 137–150. [[CrossRef](#)]
43. Muscheler, R.; Beer, J. Solar Forced Dansgaard/Oeschger Events? *Geophys. Res. Lett.* **2006**, *33*, 12–15. [[CrossRef](#)]
44. Conant, R.T.; Ryan, M.G.; Ågren, G.I.; Birge, H.E.; Davidson, E.A.; Eliasson, P.E.; Evans, S.E.; Frey, S.D.; Giardina, C.P.; Hopkins, F.M.; et al. Temperature and Soil Organic Matter Decomposition Rates—Synthesis of Current Knowledge and a Way Forward. *Glob. Chang. Biol.* **2011**, *17*, 3392–3404. [[CrossRef](#)]
45. Kutzbach, J.E.; Liu, X.; Liu, Z.; Chen, G. Simulation of the Evolutionary Response of Global Summer Monsoons to Orbital Forcing over the Past 280,000 Years. *Clim. Dyn.* **2008**, *30*, 567–579. [[CrossRef](#)]
46. Webster, P.J. The Role of Hydrological Processes in Ocean-Atmosphere Program in Atmospheric and Oceanic Sciences. *Rev. Geophys.* **1994**, *32*, 427–476. [[CrossRef](#)]